JOURNAL OF MATERIALS SCIENCE 28 (1993) 835–846

Dislocation-induced damping in metal matrix composites

J. ZHANG, R. J. PEREZ, E. J. LAVERNIA
Materials Science and Engineering, Department of Mechanical and Aerospace Engineering, University of California, Irvine, CA 92717, USA

The damping response of crystalline metals and alloys is generally associated with the presence of defects in the crystal lattice. The disturbance of these defects, usually in response to an applied cyclic load, dissipates energy, a mechanism known as "internal friction". The various defects commonly found in crystalline materials include point defects (e.g. vacancies), line defects (e.g. dislocations), surface defects (e.g. grain boundaries) and volume defects (e.g. inclusions). Among these, dislocations are noteworthy because they play a critical role, not only in the damping response of crystalline materials, but also in the overall mechanical behaviour of the materials. Among the various structural materials actively being developed, metal matrix composites (MMCs) have received considerable attention as a result of their potential to combine reinforcement properties of strength and environmental resistance, with matrix properties of ductility and toughness. Of interest is the generally observed phenomenon that MMCs exhibit unusually high concentrations of dislocations, an observation typically attributed to the difference in coefficient of thermal expansion between matrix and reinforcement. The objectives of the present paper are to provide an overview of the sources of dislocation generation in MMCs, and to provide insight into the effects that dislocations have on the damping response of MMCs. The presence of dislocations in MMCs is highlighted on the basis of transmission electron microscopy studies, and the dislocation damping mechanisms are discussed in light of the Granato–Lücke theory.

1. Introduction

Metal matrix composites (MMCs) are a unique class of materials consisting of a reinforcing phase embedded in an alloy or metal matrix. The reinforcements are typically ceramic materials (although metals may also be used), such as Al_2O_3, B_4C, SiC, Al_3N_4, and graphite, and they may be present in the form of continuous and discontinuous fibres, flakes, or particulates. The incorporation of a ceramic phase into a metal matrix leads to a series of advantages and disadvantages [1–8]. The advantages include: improved creep and fatigue behaviour, wear resistance, and a reduced coefficient of thermal expansion (CTE). The disadvantages include: reduced ductility, less than optimum fracture toughness, decreased specific heat capacity and poor machinability.

The processing techniques used to fabricate MMCs may be loosely classified into three categories [3, 4], depending on the thermal history of the matrix, as liquid, solid, and semi-solid processes. Liquid-phase processes, for example casting, typically involve the addition of reinforcements to fully molten matrix; these processes have reached an advanced stage of development, and are actively used in a series of applications [9–12]. In solid-phase processing, the temperature of the matrix during processing rarely exceeds the solidus temperature. This approach involves blending a matrix, in particulate form (e.g. powders) with a reinforcing phase, under elevated temperatures and pressures [13–15]. Semi-solid processes are perhaps at their infancy in terms of development, and involve mixing the reinforcing phases under thermodynamic conditions such that the matrix contains both solid and liquid; these include rheocasting [16–18] and spray atomization and deposition processes [19–21].

An important microstructural characteristic frequently reported for MMCs, processed by a variety of techniques, is the presence of a well-defined dislocation network in the vicinity of the reinforcement/matrix interface [22–27]. The origin of these dislocations [23–26] is generally attributed to the difference in the CTE of the metal matrix (CTEs for commonly used metals in MMCs typically range from 20–30 $\times 10^{-6}\,°C^{-1}$; see Table I) and that of the ceramic reinforcements (typically $1-10 \times 10^{-6}\,°C^{-1}$; see Table I). As the temperature of MMC decreases from near the melting point of the matrix during processing, the large difference in CTEs between reinforcement and matrix leads to the development of high stresses in the matrix region surrounding the ceramic phase. These high residual stresses are partially relieved during cooling by the generation of prismatic dislocations. Experimental support to this mechanism has

0022–2461

TABLE I Thermomechanical behaviour of typical matrices and reinforcements [43, 64, 71–74]

Materials	σ_{ys} (MPa)	E (GPa)	CTE ($10^{-6}\,°C^{-1}$)	Q^{-1} (10^{-3})
Al	10–35	70	23.6	0.05–2.5
6061-0 Al	55	70	23.4	1.0–2.0
6061-T6 Al	275	70	23.4	2.5–5
Mg	27–69	45	27.0	14–60
AZ31 Mg	131	45	26.0	0.04–10
Al_2O_3	276	360	7.2–8.6	0.01–1.0
BN	860	900	4.8–5.8	28–40
B_4C	300	450	5.0	–
Graphite (C)	1860	690	– 1.4–27.0	10–15
SiC	500	440	4.3–5.6	1.1–2.5

been established on the basis of results from neutron diffraction studies [28, 29], and from differences in tensile and compressive mechanical properties [30]. Furthermore, the presence of a high dislocation density in the vicinity of the reinforcement/matrix interface has been experimentally observed using etch pit and slip line techniques [31–33], high-resolution transmission optical microscopy [27, 34–37], as well as transmission electron microscopy (TEM) [22–26, 38–42]. The results of these studies revealed a variety of dislocation configurations surrounding the reinforcing phase, including long dislocations along fibres [39], dislocations emitted at whisker ends and corners [40, 42] as well as various loops and tangles [22, 38]. The implications of these dislocations in the mechanical behaviour of MMCs have been studied extensively and are now known to be responsible for damping [43–52], strengthening [53–55], accelerated ageing [56, 57], and improved creep behaviour [58].

While a large body of research work has been concentrated on the strengthening effects of dislocations in MMCs [53–55, 59–63], the effect of dislocations generated due to the thermal strain mismatch on the damping of MMCs have not received much attention. Material damping is a mechanism of energy dissipation allowing unwanted vibration in structures to be reduced without the use of external dampers. The damping in crystalline materials can be attributed to several mechanisms such as thermoelastic damping, magnetic damping, viscous damping and defect damping [43–47]. The first three types of damping mechanisms result from the bulk response of a material and are classified as extrinsic sources. Defect damping, an intrinsic source, stems from the internal friction resisting atomic movement in the regions of microstructural defects in crystalline metals and alloys. To some extent these imperfections alter the otherwise perfect symmetry and uniformity of the metallic crystal structure. It is these discontinuities that govern the microstructural deformation behaviour of a material under applied load, and therefore dominate the macromechanical behaviour of the material in service. Of the aforementioned defects, dislocations are particularly noteworthy because they play a critical role in the damping response of crystalline materials [45–49].

The objectives of the present paper are to (a) discuss the recent findings related to the sources of dislocation generation in MMCs, and (b) provide insight into the effects of dislocations on the damping response of MMCs. First, the mechanisms of dislocation generation in MMCs due to thermal mismatch are discussed using the experimental results from *in situ* transmission electron microscopy (TEM) observations by Vogelsang *et al.* [22], Arsenault and Shi [23], and from transmission optical microscopy by Dunand and Mortensen [27, 34–37]. Second, the damping mechanisms in crystalline materials such as metals, alloys and ceramics are succinctly summarized. Defect damping mechanisms in MMCs, and the relationship between dislocations and damping behaviour, are systematically discussed on the basis of the Granato–Lücke dislocation damping theory [47–49]. Finally, a number of examples derived from the results of Wolfenden and Wolla [50, 51], Hartman *et al.* [52], Rawal *et al.* [64] and Umekawa *et al.* [65] are discussed to highlight dislocation damping in MMCs.

2. Generation of dislocations in MMCs by thermal mismatch

2.1. Thermal mismatch strains

The thermal mismatch effect results from the deformation constraints that are present between constituents with different CTEs. As early as the 1950s, Hedges and Mitchell [66] noted that dislocations could be generated from the interface of a misfitting particle and a ductile matrix. Weatherly [67] found that in a SiO_2/Cu alloy, multiple dislocation tangles were present around SiO_2 and attributed this phenomenon to the difference in CTEs between Cu and SiO_2. Chawla and Metzger [31, 32], using an etch-pitting technique, observed that in Cu–W alloy the dislocation density was much higher at the Cu/W interface than in the bulk matrix. Similar results have also been reported by other investigators [68–70].

In MMCs, the CTE values of metal matrices are approximately $25 \times 10^{-6}\,°C^{-1}$ and those for ceramic reinforcements are approximately $5 \times 10^{-6}\,°C^{-1}$ (Table I). The CTE values shown in the table indicate that the differences in CTEs between the metal matrices and ceramic reinforcements fall into a range $10–20 \times 10^{-6}\,°C^{-1}$. It is expected that such a large difference in CTEs between matrices and reinforcements could generate a high density of dislocations during solidification of the MMCs. The residual strain, or strain

accumulation, produced as a result of the thermal mismatch, may be calculated from [1]

$$\varepsilon = \Delta\alpha \Delta T \quad (1)$$

where ΔT is the temperature change during solidification of MMCs and $\Delta\alpha$ is the difference between the CTEs of reinforcement and matrix. Because of the thermal mismatch strains, the matrix in the region adjacent to ceramic reinforcements experiences a residual stress concentration [23]. If the thermal strain is high enough, the matrix yields, and the ensuing plastic flow leads to the formation of a dislocation network in the matrix adjacent to reinforcement/matrix interface as a result of partial release of the residual stress. In an SiC whisker-reinforced 6061 Al MMC, for example, the whisker and matrix are generally processed at 700 °C and then allowed to cool to room temperature. The temperature difference, ΔT, during the cooling is approximately 675 °C. By substituting the ΔT and CTE values for SiC and 6061 Al alloy (Table I) into Equation 1, it is found that the thermal mismatch strain at the SiC/Al interface is approximately equal to 1.24%. The estimated stress in the 6061 Al matrix under this strain is approximately 870 MPa, which is much higher than the yield strength of 6061 Al alloy, 270 MPa (Table I). Hence, plastic deformation of the matrix will take place.

2.2. Generation and observation of dislocations

The presence of an elevated concentration of dislocations in the matrix region adjacent to the reinforcement/matrix interface in MMCs has been documented by a number of investigators using etch pits, slip lines, as well as *in situ* TEM experiments. All these experimental techniques, particularly TEM technique, have revealed a variety of dislocation configurations surrounding the reinforcing phase, including long dislocations along fibres, dislocations emitted at whisker ends and corners as well as various loops and tangles. In *in situ* TEM observations, the sample is examined on a thermal stage that can heat and cool the TEM sample. Hence, the microstructural changes during cooling in the *in situ* studies simulate those during MMC processing.

Vogelsang *et al.* [22] investigated dislocation generation in the matrix region adjacent to the Al/SiC interface on cooling an SiC whisker-reinforced 6061 Al alloy MMC with a whisker volume fraction of 20% under thermal cycling by using *in situ* TEM. Fig. 1 shows dislocation generation in the region adjacent to SiC whiskers that are perpendicular to the TEM foil surface at different temperatures during a heating and cooling cycle. As is evident from the figure, dense dislocation networks were present in the matrix near an SiC whisker at low temperatures. As the MMC sample was heated, dislocations appeared to undergo both straightening and rearrangement, eventually decreasing in density. As the MMC was cooled from the maximum temperature (530 °C), the dislocation density, continuously increased, until it attained the original level at approximately 100 °C (i.e. the level present at room temperature prior to the experiments). Fig. 2 shows dislocation generation in the region adjacent to SiC whiskers that are parallel to the TEM foil surface at different temperatures during a thermal cycle. The same dislocation changes as in Fig. 1 were observed. The density of dislocations present in the MMCs at room temperature was estimated to be 10^{14} m^{-2} and was attributed to the difference in CTEs between metal matrix and ceramic reinforcement during cooling [22]. These observations are consistent with the results anticipated from Equation 1, which suggests that as ΔT decreases, the residual strain also decreases with a concomitant reduction in the dislocation density. It was thought that the dislocations were produced by differential thermal contraction of aluminium and SiC on cooling from the elevated temperatures of annealing.

Arsenault and Shi [23] recorded a series of TEM images of a platelet SiC/6061 Al MMC and calculated the density of dislocations, ρ, from the following equation

$$\rho = \frac{2n}{Lt} \quad (2)$$

where n is the number of dislocations intersecting the grid lines, L the length of the grid lines divided by the magnification, and t the thickness of the TEM foil sample. The observed value, 10^{14} m^{-2}, of the dislocations in the MMC by TEM agreed well with the value of 10^{13} m^{-2} calculated from [22, 75]

$$\rho = \frac{\varepsilon_p}{\boldsymbol{b} L_a} \quad (3)$$

where ε_p is the plastic strain (1% was used), L_a the average distance moved by the generated dislocations (2 μm was used) and $\boldsymbol{b}$ the Burgers vector of the 6061 Al matrix ($\boldsymbol{b}$ = 0.3 nm was used).

Arsenault and Shi [23] also noted that these results were consistent with those anticipated from a theoretical model involving the prismatic punching of dislocations at a ceramic particle as determined by

$$\rho = \frac{B\varepsilon V_f}{\boldsymbol{b} t(1 - V_f)} \quad (4)$$

where ε is the thermal mismatch strain given by Equation 1, V_f is the volume fraction of the ceramic reinforcement, $\boldsymbol{b}$ the Burgers vector, t the smallest dimension of the reinforcement and B the geometric constant (between 4 for particulates with one dimension very small compared with the other two, and 12 for equiaxed particulates). Generally, V_f ranges from 5%–50%, t falls in the micrometre range (1–15 μm), $\boldsymbol{b}$ is 0.3 nm, and ε is around 1%. Substituting these values into Equation 4, ρ is estimated to be 10^{13}–10^{14} m^{-2}, which is consistent with TEM results. However, the dislocation prismatic punching model fails when V_f is equal to zero, because Equation 4 gives zero dislocation density for unreinforced metals and alloys, which is not the case in metals and alloys.

As a comparison, Fig. 3 shows a micrograph of an unreinforced 6061 Al control sample illustrating low dislocation density as well as large grain size [22].

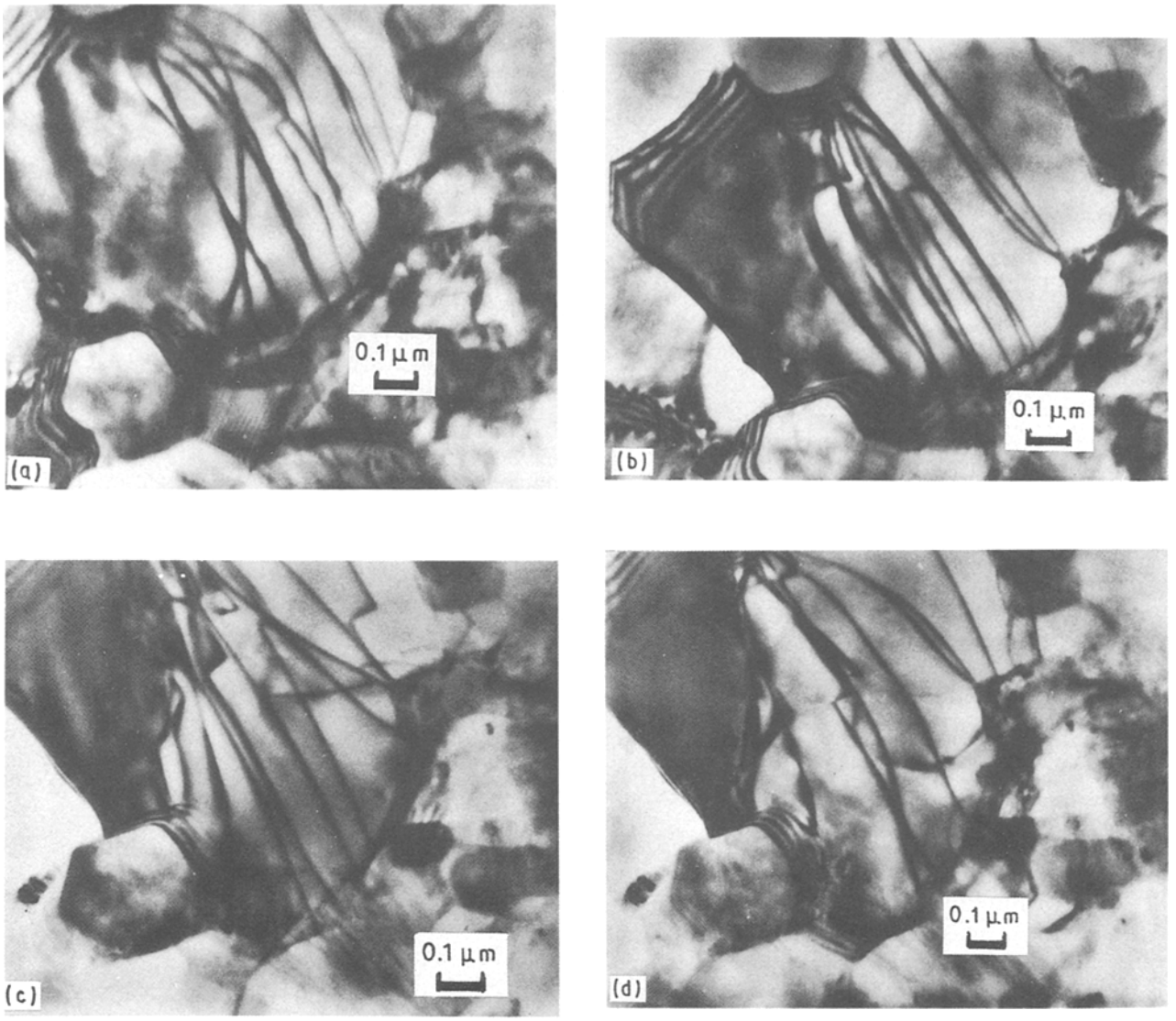

Figure 1 Dislocation generation in the matrix region adjacent to SiC whisker at different temperatures during the thermal heating and cooling cycle [22]. (a) 100 °C, heating; (b) 300 °C, heating; (c) 530 °C, maximum; (d) 300 °C, cooling, (e) 90 °C, cooling.

Fig. 3a shows few dislocations in the control sample that were thought to be associated with second phases (precipitate). Fig. 3b shows a large precipitate surrounded by dislocations at the beginning of the thermal cycle (70 °C). Fig. 3c demonstrates that as temperature was increased to the annealing temperature in the TEM (500 °C), the dislocations gradually disappeared until only a few remained. During *in situ* cooling of the control sample, dislocations reformed in the vicinity of the precipitate whereas most of the matrix remained free of dislocations.

Dunand and Mortensen [27, 34–37] used a glass particle/silver chloride (glass/AgCl) transparent composite as an analogous MMC to observe CTE mismatch generated dislocations using the decoration technique and high-resolution transmission optical microscopy. The glass/AgCl behaves similarly to MMCs and exhibits dislocation mechanisms which are, in most cases, similar to those found in metals. The use of the glass/AgCl model material avoids the shortcomings associated with TEM observations in metals containing reinforcements of large size. The stress-relief process due to the thermal mismatch involved the generation of rows of prismatic loops or tangles of dislocations, forming a well-defined surrounding plastic zone. According to Dunand and Mortensen [35], the size of the plastic zone is given by

$$c_s = r_s\left(\frac{\varepsilon E}{(1-\nu)\sigma_{ys}}\right)^{1/3} \quad \text{around a spheroidal particle} \qquad (5)$$

$$c_c = r_c\left(\frac{4\varepsilon E}{(5-4\nu)\sigma_{ys}}\right)^{1/2}$$

around a cylindrical particle (6)

where ε is the thermal mismatch strain by Equation 1, r_s and r_c the spheroidal and cylindrical particle radii, E, ν, and σ_{ys} are Young's modulus, Poisson's ratio and yield strength of the matrix. The dislocation density in the bulk matrix was estimated from

$$\rho_s = \frac{6\sqrt{2}\,\varepsilon}{\boldsymbol{b}(c_s^3 - r_s^3)/r_s} \quad \text{for a spheroidal particle} \quad (7)$$

$$\rho_c = \frac{2\sqrt{2}\,\varepsilon}{\boldsymbol{b}(c_c^2 - r_c^2)/r_c} \quad \text{for a cylindrical particle} \quad (8)$$

where $\boldsymbol{b}$ is the Burgers vector. By simulating the plastic zones in the AgCl matrix and metal matrix and comparing thermomechanical properties of constituents of the glass/AgCl model material and MMCs, it was found that the dislocation density in a 99.5% pure aluminium containing 1.5 μm SiC particles was around 10^{12}–10^{13} m^{-2}, which is consistent with other observations [22, 52].

Dislocations generated due to thermal mismatch strain in MMCs have also been investigated by other investigators [24, 25, 38–42]. In summary, the results cited in this section demonstrate, first, that the high density of dislocations that is reportedly present in most MMCs may be rationalized on the basis of the difference in CTEs between metal matrix and ceramic reinforcement, and second, that these dislocations are generated by a prismatic punching mechanism during cooling from elevated processing temperatures.

3. Characterization of damping capacity of materials

Material damping is related to time-dependent elasticity. Elasticity theory of crystalline metallic materials dictates that the relationship between an applied load and the resultant deformation obeys Hooke's Law, i.e. the resultant strain is proportional to the applied stress. Hooke's law, however, does not account for the time effect, that is, the applied load and the resultant deformation are assumed to be perfectly in phase, a condition only valid when the loading rate is so low that the deformation process may be considered to be an instantaneous, and therefore a static one. In practice, metals and alloys respond to an applied load not only by an instantaneous elastic strain that is time-independent, but also by a lag strain behind the applied load, which is time dependent [44]. Therefore, the overall strain, ε, consists of two parts; one part, ε_e, is the elastic strain, and the other, ε_a, the anelastic strain, i.e.

$$\varepsilon = \varepsilon_e + \varepsilon_a \quad (9)$$

$$\varepsilon_a = \varepsilon_i[1 - \exp(-\tfrac{t}{\tau})] \quad \text{for loading} \quad (10)$$

$$\varepsilon_a = \varepsilon_i \exp(-\tfrac{t}{\tau}) \quad \text{for unloading} \quad (11)$$

where ε_i is the initial strain, t is the time and τ is the characteristic relaxation constant which characterizes the magnitude of internal friction or damping of a material. Because of the lag induced by the relaxation, the stress versus strain curve forms a hysteresis loop when the material is under cyclic loading. The area enclosed by the hysteresis loop represents the energy dissipated inside the material during one cycle. Such dynamic hysteresis at low stress levels is defined as anelasticity or damping. There are several quantities which can be used to characterize internal friction or damping capacity. Usually, specific damping capacity (SDC), ψ, the ratio of the dissipated energy to the maximum stored energy of one complete cycle, is used to characterize damping capacity [43]

$$\psi = \frac{\Delta W}{W} \quad (12)$$

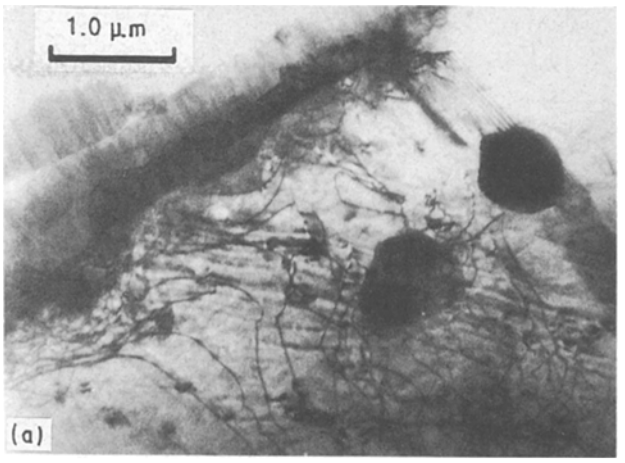

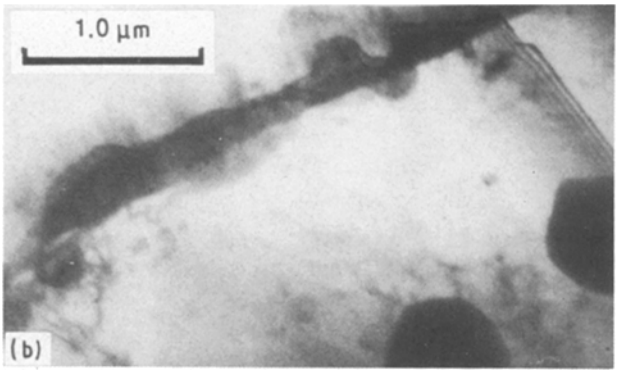

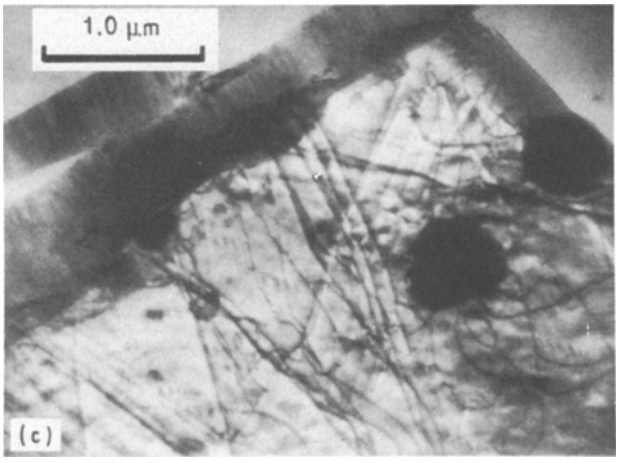

Figure 2 Dislocation generation in the matrix region adjacent to SiC whisker, TEM foil sectioned parallel to the SiC whisker [22]. (a) 70 °C, heating; (b) 540 °C, maximum; (c) 130 °C, cooling.

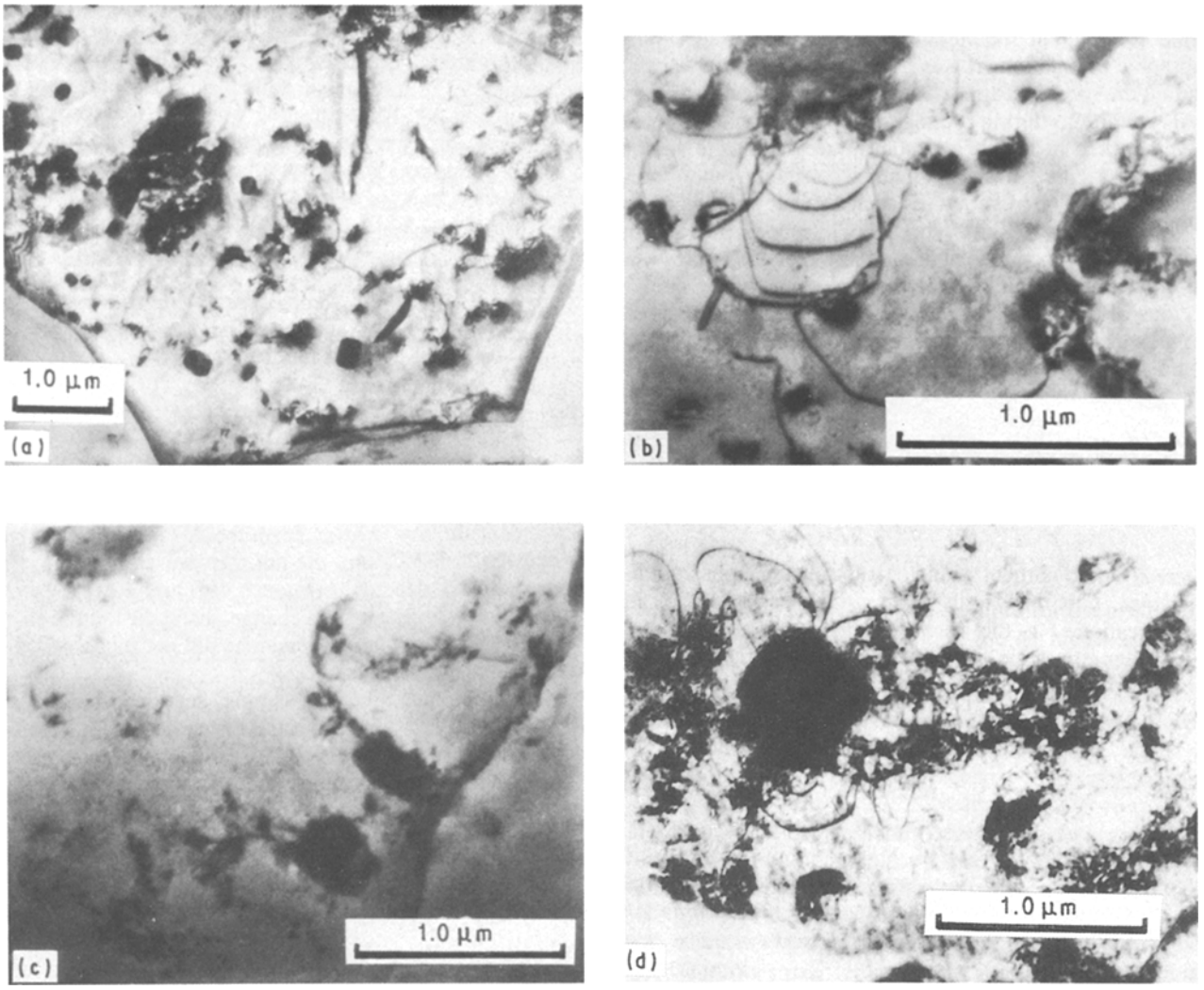

Figure 3 Micrograph of a 6061 Al control sample illustrating (a) the low dislocation density and the large grain size, (b) dislocation around a precipitate at 70 °C, heating, (c) disappearance at 510 °C, maximum and (d) reappearance of dislocation at 100 °C after cooling [22].

where

$$\Delta W = \oint \sigma \, d\varepsilon \tag{13}$$

$$W = \int_{\omega t = 0}^{\omega t = \pi/2} \sigma \, d\varepsilon \tag{14}$$

where σ and ε are the cyclic stress and strain, respectively, and they are expressed by [50]

$$\sigma = \sigma_0 \exp(i\omega t) \tag{15}$$

$$\varepsilon = \varepsilon_0 \exp[i(\omega t - \phi)] \tag{16}$$

where σ_0 and ε_0 are the stress and strain amplitude, respectively, $\omega = 2\pi f$ is the circular frequency and f the vibration frequency, and ϕ is the loss angle by which the strain lags behind the stress (Fig. 4b). In an ideally elastic material, $\phi = 0$ and $\sigma/\varepsilon = E$, the elastic modulus in Hooke's law. However, most materials are anelastic, so ϕ is not zero and the ratio is complex. The resultant complex modulus is defined as

$$E = \frac{\sigma}{\varepsilon}$$

$$= \frac{\sigma_0}{\varepsilon_0}(\cos\phi + i\sin\phi)$$

$$= E' + iE'' \tag{17}$$

where

$$E' = \frac{\sigma_0}{\varepsilon_0}\cos\phi \tag{18}$$

is the storage modulus, and

$$E'' = \frac{\sigma_0}{\varepsilon_0}\sin\phi \tag{19}$$

is the loss modulus. The ratio of the two moduli gives

$$\eta = \frac{E''}{E'}$$

$$= \tan\phi \tag{20}$$

where η is the loss factor and $\tan\phi$ the loss tangent. The loss tangent is related to the relaxation time, τ, by [44]

$$\tan\phi = \frac{c\omega\tau}{1 + \omega^2\tau^2} \tag{21}$$

where c is the physical constant. Therefore, $\tan\phi$ is a measure of the energy dissipated in a material during cyclic loading.

Logarithmic decrement is another damping quantity and is derived from amplitude decay of a specimen

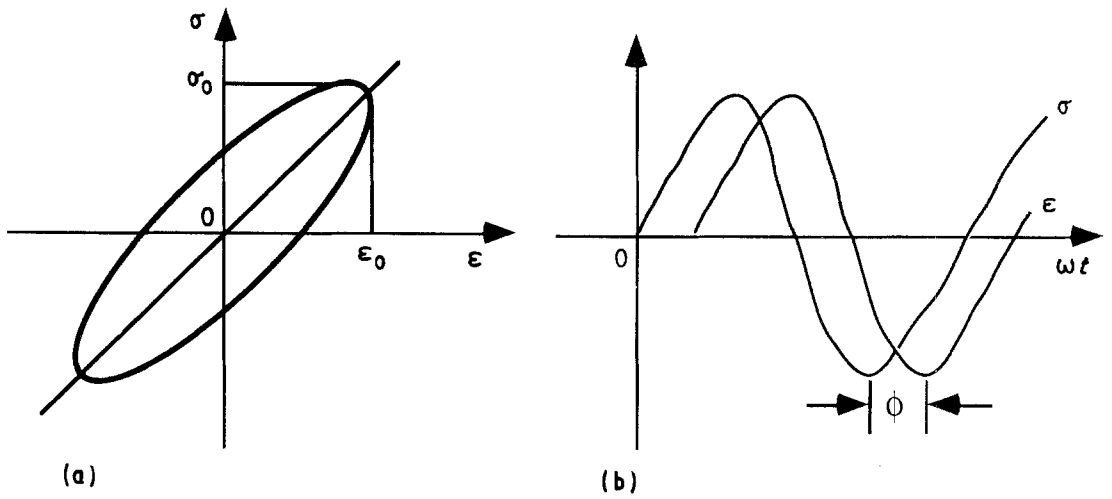

Figure 4 Stress–strain hysteresis and phase lag of anelastic materials. (a) Stress–strain hysteresis, (b) cyclic stress and strain.

under free vibration. An anelastic material in vibration can be analogized by the one-dimensional vibration response of a linear mechanical system with a spring (restoring force), a mass point and a dashpot resistance (damping). Logarithmic decrement, δ, is given by [46]

$$\delta = \frac{1}{n}\ln\left(\frac{A_i}{A_{i+n}}\right) \tag{22}$$

where A_i and A_{i+n} are the amplitudes of the ith cycle and the $(i + n)$th cycle, at times t_1 and t_2, respectively, separated by n periods of oscillation.

In addition to SDC, loss factor, loss tangent, and logarithmic decrement, the inverse quality factor, Q^{-1}, is also widely used to characterize material damping through [44]

$$Q^{-1} = \frac{f_2 - f_1}{f_r} \tag{23}$$

where f_1 and f_2 refer to half-power bandwidth frequencies and f_r the resonant frequency in the spectrum of square amplitude versus frequency for a specimen under forced vibration. The broadness of the resonant peak characterizes the magnitude of material damping. In materials exhibiting low damping levels (e.g. $\tan\phi < 0.1$), such as metals and alloys, all of the aforementioned damping quantities, ψ, δ, $\tan\phi$, ϕ, and Q^{-1}, are related by [76]

$$\begin{aligned}\psi &= 2\delta \\ &= 2\pi\tan\phi \\ &= 2\pi\phi \\ &= 2\pi Q^{-1}\end{aligned} \tag{24}$$

Among the various damping mechanisms, internal friction of defects makes a large contribution to the overall damping in crystalline materials. In a perfect single crystal under an applied stress (the stress level being well below the yield stress), every unit cell of the crystal deforms uniformly and can return to its original shape by interatomic bonding elasticity upon removal of the applied load. In an imperfect single crystal, however, each defect causes distortion of the crystal symmetry and therefore induces an accompanying stress concentration. Although the magnitude of the bulk applied stress is small, the local stress concentration may be sufficient to cause atomic rearrangement in such regions of pre-existing stress. The atoms during rearrangement can experience peripheral atomic displacements, which are essentially viscous in nature and occur in response to the applied load. The atoms in the distorted region are capable of sliding over one another in a fashion similar to polymer chains in a long-chain polymer. At high temperatures this sliding can be extensive and lead to a viscoelastic strain. At ambient temperatures, the relative atomic displacements are typically fractions of an atomic diameter. The displaced atoms may introduce internal stress relaxation and the displacements can be recovered upon load removal. This deformation mechanism leads to mechanical hysteresis.

In crystalline metals and alloys, defects are generally considered to be the primary sources for the dissipation of elastic strain energy [45–49]. Material damping manifests itself as a phase lag between an applied stress and the resulting deformation. Such a phase lag results from deformation characteristics of materials as a function of time (i.e. relaxation [46]). There are two time factors attributed to the phase lag; one is the rearrangement of atoms in a local region and the other is the deformation propagation. It is known that, macrostructurally, the attenuation and propagation of a mechanical wave are related to the uniformity of the medium in which the wave propagates. Similarly, the relaxation time of deformation in crystalline materials containing defects would be longer than in perfect crystalline materials. Therefore, it follows that the characteristic relaxation time during deformation is longer in crystalline metals containing defects than in those without defects. The presence of defects in a crystalline material breaks up the uniformity of the medium and makes it difficult for deformation to be precisely in phase with the applied load.

The damping capacity, as defined by the inverse quality factor, Q^{-1}, of various metal matrices and ceramic reinforcements commonly used in fabrication of MMCs are summarized in Table I. Inspection of the

data shown in the table reveals that the intrinsic damping capacity for aluminium and Al_2O_3 is basically small. However, Al_2O_3/Al MMC exhibits a higher damping than either of its constituents [77]. The increase in the resultant damping of the MMC is thought to be due to the thermal strain mismatch effect. A comprehensive listing of damping data for metals, alloys, ceramics, and MMCs, has recently been completed by Zhang *et al.* [72] and the interested reader is encouraged to review the literature.

4. Relationship between damping capacity and dislocations

The dissipation of elastic strain energy (e.g. damping) occurs by means of one, or a combination of the following mechanisms: defect damping, thermoelastic damping, magnetic damping, and viscous damping [43–49]. In crystalline metals and alloys, defects are generally considered to be the primary sources for dissipation of elastic strain energy; these include point defects, dislocations, grain boundaries and interfaces in general [45, 46]. As discussed in the previous section, material damping manifests itself as a phase lag between an applied stress and the ensuing deformation. Because such a phase lag depends on the deformation characteristics as a function of time, damping is similar to attenuation of wave propagation, in which the attenuation and propagation of a mechanical wave are both related to the extent of uniformity of the medium of interest. Therefore, it follows that the characteristic relaxation time during deformation is longer in crystalline materials containing defects than in those that do not contain any defects. The presence of defects in a crystal breaks up the uniformity of the medium, and makes it difficult for deformation to be precisely in phase with an applied load.

The presence of dislocations in a crystalline lattice may influence damping by two mechanisms [50]. First, the relative movements of the atoms are more easily initiated in the dislocation regions than in the dislocation-free regions. The movements of the atoms in defect material, on the other hand, are resisted by internal friction from neighbouring lattice, and therefore, lead to extra sources of energy dissipation. Second, the presence of dislocations interferes with the homogeneous propagation of deformation, thereby increasing the phase lag between applied load and deformation. The first mechanism is operative as the movement of dislocations is generally impeded by the presence of point defects, precipitates, and other out-of-plane dislocations. Although early studies on the internal friction effects in cold-worked lead, copper, silver and aluminium [78–80] had recognized the important role that dislocations played in the dissipation of elastic strain energy, it was not until 1956 that a formal theory was proposed by Granato and Lücke [47]. This theory was developed by Granato and Lücke on the basis of Koehler's analogy model [80], and therefore became known as the Koehler–Granato–Lücke (KGL) theory, or more commonly as the Granato–Lücke (GL) theory [47–49, 81–83].

In the GL dislocation model, the dislocation line is likened to an elastically vibrating string fixed at the pinning points in the crystal lattice, as schematically illustrated in Fig. 5. Under the applied cyclic loading, the dislocation line extends out from the fixed points produced by pinning impurity atoms, precipitates or antiplane dislocations. As the applied stress amplitude is increased, the pinned dislocation may bow out at some weak pinning points and thereafter the further motion of the dislocation line undergoes a higher vibration amplitude. The motion of the dislocation depends on the local stress field adjacent to the dislocation. For low-frequency ranges (kHz), the loss

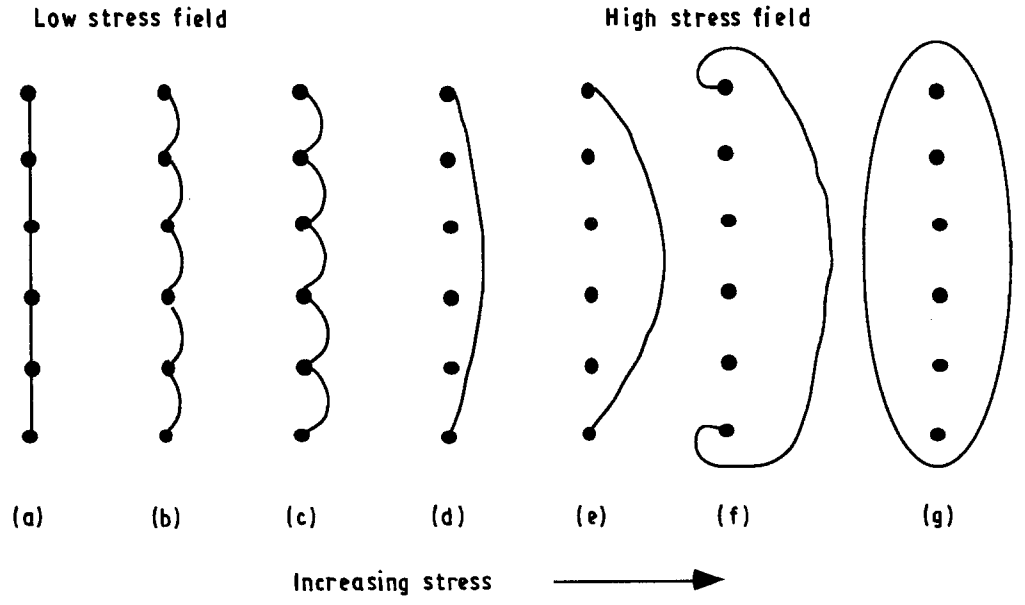

Figure 5 Granato–Lücke vibration string model [47].

factor, Q^{-1}, is given by

$$Q^{-1} = Q_a^{-1} + Q_f^{-1} \quad (25)$$

where

$$Q_a^{-1} = C_1 \frac{\rho \boldsymbol{b}^2}{\varepsilon_0} \exp\left(-\frac{C_2}{\varepsilon_0}\right) \quad (26)$$

and

$$Q_f^{-1} = C_3 \rho f^2 / \boldsymbol{b}^2 \quad (27)$$

where C_1, C_2 and C_3 are physical constants, ρ and $\boldsymbol{b}$ are dislocation density and Burgers vector, respectively; ε_0 and f are vibration strain amplitude and frequency, respectively. Q_f^{-1} is called the frequency-dependent part and Q_a^{-1} the amplitude-dependent part. From these equations, it is evident that dislocation damping is proportional to dislocation density and the square of Burgers vector. Both ρ and $\boldsymbol{b}$ can be determined using transmission electron microscopy and other microstructural characterization techniques, whereas C_1, C_2, C_3 and ε_0 depend on the specific experimental parameters and the specimen physical constants [47, 48]. C_1, C_2 and C_3 are given by the following definitions

$$C_1 = \frac{\omega \Delta_0 L_N^3 K \rho_m \varepsilon'}{\delta \pi \omega_r L_c^2} \quad (28)$$

$$C_2 = \frac{K \varepsilon' a}{L_c} \quad (29)$$

$$C_3 = \frac{\pi^2 B \Delta_0^2 L_e^4}{2 \delta \omega_r G} \quad (30)$$

$$K = \frac{32G}{\pi^2 p^2 RE} \quad (31)$$

$$\Delta_0 = \frac{4(1-\nu)}{\pi^2} \quad (32)$$

where ω and ω_r are angular frequency and resonant frequency; L_N is the dislocation network length that depends on the interfibre or interparticle spacing in the cases of MMCs, L_c the minor pinning length that is 0.02–2 μm suggested for MMCs by Wolfenden *et al.* [84], and L_e the effective loop length equal to 3.3 L_c; ρ_m is the matrix material mass density; ε' is Cottrell's misfit parameter that is equal to the fractional difference in the size of the solute and solvent atoms and was suggested to be 10^{-2} by Granato and Lücke [47]; a is the lattice parameter; E, G and ν are Young's and shear moduli and Poisson's ratio of the matrix, respectively; p is the constant between 2 and 3; R is the resolved shear stress factor by Schmid's principle; B is a constant of 5×10^{-5}–5×10^{-3} [47].

One of the characteristics of dislocation damping is its strain-amplitude dependency. This dependency has been demonstrated in several MMC systems [51, 52, 64, 65, 84]. Fig. 6 shows the amplitude dependence of material damping of SiC_p/6061 Al MMC with a volume fraction of 5% [52]. The shape of the curve obtained when internal friction is plotted versus strain amplitude, as shown in Fig. 6, is one of the characteristics of dislocation-induced damping. This type of plotting can be used to judge whether or not dislocation damping is present in a material. It is noted that at low strain amplitudes, MMC damping mainly results from the frequency-dependent part, Q_f^{-1}, and beyond a critical strain amplitude, the strain amplitude-dependent part, Q_a^{-1}, becomes dominant. The occurrence of the critical strain amplitude is correspondent to the break-away of pinned dislocation line (Fig. 5d) [47]. From Equations 25 to 27, it follows that one possible way to increase the damping capacity of a material is to increase the density of dislocations present. It then follows that MMCs should exhibit a relatively high damping capacity, as a result of the high density of dislocations present in these MMCs.

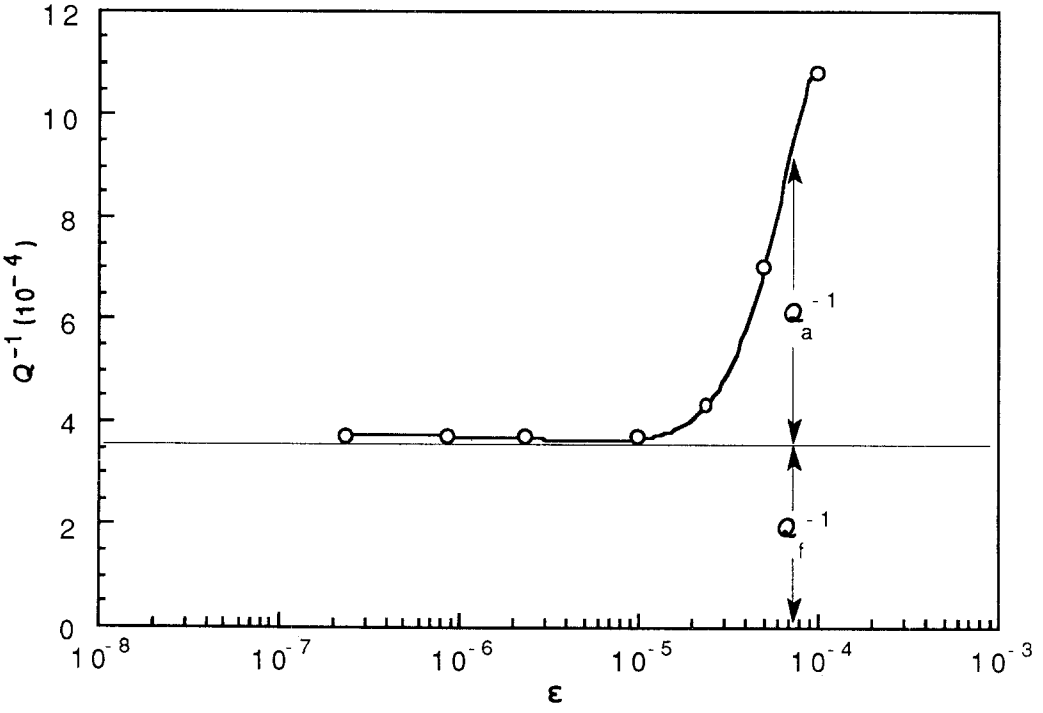

Figure 6 Damping dependence of 6061 Al/SiC_p on strain amplitude and frequency [52].

Umekawa *et al.* [65] investigated the changes in the damping dependency in SiC whisker-reinforced Al MMCs as the volume fraction of the SiC whiskers was varied. It was found that as the volume fraction was increased from 0%, 12%, 15% and 22% the critical strain amplitude shifted from 0.3×10^{-3} to 1.0×10^{-3} and at the same time the strain amplitude-dependent damping was suppressed in MMCs containing a high volume fraction of SiC whiskers. Unfortunately, in Umekawa's studies, no dislocation density data were reported.

Rawal *et al.* [64] investigated the damping behaviour of unidirectional P55 carbon fibre-reinforced 6061 Al MMCs. The GL theoretical analysis of their results yielded mobile dislocation densities of $10^{13}\ m^{-2}$ that corresponded with the measured average dislocation density of $10^{14}\ m^{-2}$ in the interfibre matrix region determined by TEM images [22]. It was concluded that dislocation damping was the dominant mechanism in the strain-amplitude dependent region.

The Granato–Lücke theory can also be used to determine dislocation density by measuring damping capacity at different strain amplitudes. Taking the natural logarithm of both sides of Equation 26 gives

$$\ln(Q_a^{-1}\varepsilon_0) = \ln(C_1\rho b^2) - \frac{C_2}{\varepsilon_0} \quad (33)$$

Theoretically, a curve of $\ln(Q_a^{-1}\varepsilon_0)$ versus ε_0^{-1} defined by Equation 33 should be a straight line (Fig. 7). The dislocation density, ρ, can be readily determined from the intercept of the curve. Table II tabulates the dislocation density results of several particulate-reinforced aluminium alloy MMCs obtained by this methodology [52]. From the results shown in the table, as the SiC volume fraction increases, the dislocation density exhibits a slight change. It may be inferred from the observation that the damping capacity of SiC/Al MMCs may not increase with increasing volume fraction of reinforcement, beyond a certain critical value. Furthermore, from Hartman *et al.* [52], although the Granato–Lücke theory gave a reasonable prediction of dislocation densities for MMCs, it overestimated dislocation density of unreinforced aluminium alloy [56, 57, 85].

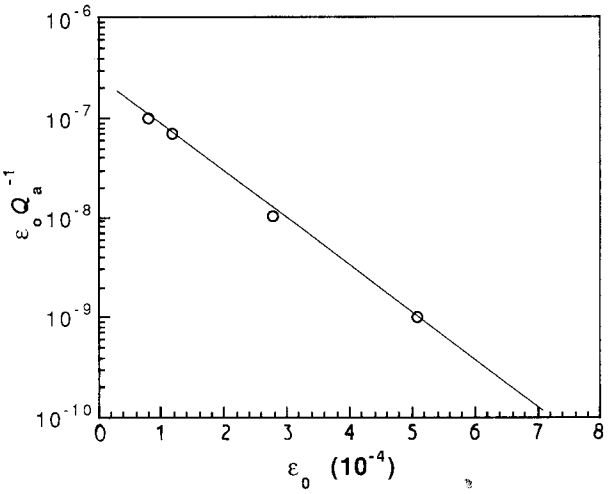

Figure 7 Curve fitting of damping capacity versus strain amplitude [52].

TABLE II Dislocation density of Al/SiC_p MMCs by damping measurement [52]

Matrix	V_f of SiC_p (%)	Dislocation density ($10^{13}\ m^{-2}$)
6061 Al	0	3
6061 Al	5	70
6061 Al	20	80
1100 Al	0	5
1100 Al	5	5
2124 Al	15	30

5. Conclusion

The high density of dislocations that is generated during MMC processing as a result of the thermal mismatch between matrix and reinforcement has an important effect on the dissipation of elastic strain energy. The relationship between dislocations and material damping may be quantitatively characterized by the Granato–Lücke theory. From the work reviewed in the present paper, it may be noted that the Granato–Lücke theory is a possible way for predicting damping capacity of a material in which dislocation damping is dominant, checking whether the dislocation damping mechanism is dominant, as well as estimating dislocation density. The verification of the dislocation damping mechanism may be accomplished by changing strain amplitude or changing dislocation density (for example, heating the MMC sample to reduce dislocation density due to thermal mismatch) or by checking the linearity of experimental data. However, careful attention must be paid in applying this theory because the quantitative analysis involves a number of materials constants requiring tedious microstructure studies.

Acknowledgement

The authors thank the Office of Naval Research of the United States (Grant no. N00014-90-J-1923) for financial support, and Catherine Wong; David Taylor Research and Development Center, Annapolis, MD, for her able technical advice and assistance and valuable discussions.

References

1. M. TAYA and R. J. ARSENAULT, "Metal Matrix Composites: Thermomechanical Behaviour" (Pergamon Press, Oxford, 1989) pp. 1–108.
2. R. K. EVERETT and R. J. ARSENAULT, "Metal Matrix Composites: Processing and Interfaces" (Academic Press, Boston, 1991).
3. T. S. SRIVATSAN, I. A. IBAHIM, F. A. MOHAMED and E. J. LAVERNIA, *J. Mater. Sci.* **26** (1991) 5965.
4. I. A. IBAHIM, F. A. MOHAMED and E. J. LAVERNIA, *ibid.* **26** (1991) 1137.
5. "Spray Deposition High Performance Materials: Metal Matrix Composites", Research and Development Report,

Alusuisse-Lonza Service Ltd, Neuhausen, Switzerland, June 1990.
6. A. L. GEIGER and J. A. WALKER, *J. Metals* **43** (8) (1991) 8.
7. A. KELLY, in "Cast Reinforced Metal Composites", edited by S. G. Fishman and A. K. Dhingra (ASM International, Materials Park, OH, 1988) pp. 1–5.
8. S. J. HARRIS, *Comp. Sci. Tech.* **35** (1989) 99.
9. P. K. ROHATGI, R. ASTHANA and S. DAS, *Int. Metals Rev.* **31** (1986) 115.
10. R. MEHRABIAN, *Mater. Res. Soc. Symp.* **120** (1988) 3.
11. D. J. LLOYD, *Comp. Sci. Tech.* **35** (1989) 159.
12. S. RAY, *Indian J. Tech.* **28** (1990) 368.
13. H. J. RACK, in "Processing and Properties for Powder Metallurgy Composites", edited by P. Kumar, K. Vedula and A. Ritter (The Metallurgical Society of AIME, Warrendale, PA, 1987) pp. 155–68.
14. B. L. FERGUSON and O. D. SMITH, in "Metals Handbook", Vol. 7, 9th Edn (ASM International, Materials Park, OH, 1984) p. 537.
15. A. FRISCH, *Powder Metall. Int.* **21** (5) (1989) 39.
16. M. C. FLEMINGS and R. MEHRABIAN, *Trans. Amer. Foundrymen Soc.* **81** (1973) 81.
17. R. MEHRABIAN, R. G. RIEK and M. C. FLEMINGS, *Metall. Trans.* **5** (1974) 1899.
18. M. C. FLEMINGS, *ibid.* **22A** (1991) 957.
19. E. J. LAVERNIA, *SAMPLE Q.* **22** (1991) 2.
20. A. R. E. SINGER, *Mater. Sci. Engng* **A135** (1991) 13.
21. Y. WU and E. J. LAVERNIA, *J. Metals* **43** (8) (1991) 16.
22. M. VOGELSANG, R. J. ARSENAULT and R. M. FISHER, *Metall. Trans.* **17A** (1986) 379.
23. R. J. ARSENAULT and N. SHI, *Mater. Sci. Engng* **A81** (1986) 175.
24. F.-S. SHIEU and S. L. SASS, *Acta Metall. Mater.* **39** (1991) 539.
25. S. M. PICKARD and B. DERGY, *ibid.* **38** (1990) 2537.
26. R. J. ARSENAULT and R. M. FISHER, *Scripta Metall.* **17** (1983) 67.
27. D. C. DUNAND and A. MORTENSEN, *Acta Metall. Mater.* **39** (1991) 1405.
28. A. J. ALLEN, M. BURKE, M. T. HUTCHINGS, A. D. KRAWITZ and C. G. WINDSOR, in "Residual Stresses in Science and Technology", edited by E. Macherauch and V. Hauck (DGM, Oberursel, Germany, 1987) p. 151.
29. D. S. KUPPERMAN, D. S. MAJUMDAR and J. P. SINGH, *J. Eng. Mater. Tech. Trans. ASME* **112** (1990) 198.
30. R. J. ARSENAULT and M. TAYA, *Acta Metall.* **35** (1987) 651.
31. K. K. CHAWLA and M. METZGER, *J. Mater. Sci.* **7** (1972) 34.
32. *Idem, Metall. Trans.* **8A** (1977) 1680.
33. Y. FOLM and R. J. ARSENAULT, *Mater. Sci. Engng* **75** (1985) 151.
34. D. DUNAND and A. MORTENSEN, *ibid.* **A135** (1991) 179.
35. *Idem, Acta Metall. Mater.* **39** (1991) 127.
36. *Idem, Mater. Sci. Engng* **A144** (1991) 179.
37. *Idem, Acta Metall. Mater.* **39** (1991) 1417.
38. S. P. RAWAL, L. F. ALLARD and M. S. MISRA, in "Proceedings of the 6th International Conference on Composite Materials (ICCM/VI)", edited by F. L. Matthews (Elsevier Applied Science, Harlow, UK, 1986) p. 2.169.
39. S. P. RAWAL, L. F. ALLARD and M. S. MISRA, in "Interfaces in Metal Matrix Composites", edited by A. K. Dhingra and S. G. Fishman (The Metallurgical Society AIME, Warrendale, PA, 1986) p. 211.
40. M. TAYA and T. MORI, *Acta Metall.* **35** (1987) 155.
41. C. T. KIM, J. K. LEE and M. R. PLICHTA, *Metall. Trans.* **21A** (1990) 673.
42. S. R. NUTT and J. M. DUVA, *Scripta Metall.* **20** (1986) 1055.
43. B. J. LAZAN, "Damping of Materials and Members in Structural Mechanics" (Pergamon Press, Oxford, 1968) pp. 38–78.
44. C. ZENER, "Elasticity and Anelasticity of Metals" (The University of Chicago Press, Chicago, 1948) pp. 41–163.
45. R. DE BATIST, "Internal Friction of Structural Defects in Crystalline Solids" (North-Holland, Amsterdam, 1972) pp. 210–417.
46. A. S. NOWICK and B. S. BERRY, "Anelastic Relaxation in Crystalline Solids" (Academic Press, New York, 1972) pp. 130–434.
47. A. V. GRANATO and K. LÜCKE, *J. Appl. Phys.* **27** (1956) 583.
48. *Idem, ibid.* **27** (1956) 789.
49. *Idem, ibid.* **52** (1981) 7136.
50. A. WOLFENDEN and J. M. WOLLA, in "Metal Matrix Composites: Mechanisms and Properties", edited by R. K. Everett and R. J. Arsenault (Academic Press, Boston, 1991) pp. 287–328.
51. *Idem, J. Mater. Sci.* **24** (1989) 3205.
52. J. T. HARTMAN Jr, K. H. KEENE, R. J. ARMSTRONG and A. WOLFENDEN, *J. Metals* **38** (4) (1986) 33.
53. M. TAYA, K. E. LULAY and D. J. LLOYD, *Acta Metall. Mater.* **39** (1991) 73.
54. M. TAYA, *Mater. Trans. JIM* **32** (1991) 1.
55. W. S. MILLER and F. J. HUMPHREYS, *Scripta Metall. Mater.* **25** (1991) 33.
56. I. DUTTA and D. L. BOURELL, *Mater. Sci. Engng* **A112** (1989) 67.
57. *Idem, Acta Metall. Mater.* **38** (1990) 2041.
58. K-T. PARK, E. J. LAVERNIA and F. A. MOHAMED, *ibid.* **38** (1990) 2149.
59. D. S. LI, M. R. WILSNOM and D. J. DINGLEY, *Comp. Sci. Tech.* **42** (1991) 413.
60. R. T. ARSENAULT, in "Metal Matrix Composites: Mechanisms and Properties", edited by R. K. Everett and R. J. Arsenault (Academic Press, Boston, 1991) pp. 79–100.
61. S. OCHIAI and K. OSAMURA, *Metall. Trans.* **21A** (1990) 971.
62. R. M. AIKIN Jr and L. CHRISTODOULOU, *Scripta Metall. Mater.* **25** (1991) 9.
63. G. J. DVORAK, in "Metal Matrix Composites: Mechanisms and Properties", edited by R. K. Everett and R. J. Arsenault (Academic Press, Boston, 1991) pp. 1–77.
64. S. P. RAWAL, J. H. ARMSTRONG and M. S. MISRA, "Damping Characteristics of Metal Matrix Composites", AD-A213 712, May 1989.
65. S. UMEKAWA, K. NISHIYAMA and E. YAMANE, in "Proceedings of the 4th Japan–US Conference on Composite Materials", American Society for Composites (Technomic, Lancaster, 1988) pp. 138–47.
66. S. M. HEDYES and J. W. MITCHELL, *Phil. Mag.* **44** (1953) 223.
67. G. C. WEALTHERLY, *Metals Sci. J.* **2** (1968) 237.
68. M. F. ASHBY and L. JOHNSON, *Phil. Mag.* **20** (1969) 1009.
69. M. F. ASHBY, H. GELLES and L. E. TANNER, *ibid.* **19** (1969) 757.
70. J. J. WILLIAMS and G. GARMONG, *Metall. Trans.* **6A** (1975) 1699.
71. H. E. BOYER and T. L. GALL, "Metals Handbook," Desk Edn. (ASM International, Materials Park, OH, 1985) p. 61.
72. J. ZHANG, R. J. PEREZ and E. J. LAVERNIA, "Documentation of Damping Capacity of Metallic, Ceramic and Metal Matrix Composite Materials", Research Report, The University of California, Irvine (1991).
73. J. LIU and P. D. OWNBY, *J. Amer. Ceram.* **74** (1991) 674.
74. E. A. BRANDES, "Smithells Metals Reference Book", 6th Edn. (Butterworths, London, 1983) p. 14-1.
75. J. K. LEE, Y. Y. EARMME, H. I. AARONSON and K. C. RUSELL, *Metall. Trans.* **11A** (1980) 1837.
76. G. G. WREN and V. K. KINRA, "Damping of Metal Matrix Composites: Theory and Experiment", Research Report, Texas A and M University (1991).
77. C. WONG and S. HOLCOMB, "Damping Studies of Ceramic Reinforced Aluminum", Report DTRC-SME-91/15, David Taylor Research Center, Annapolis, MD, March 1991.
78. T. A. READ, *Phys. Rev.* **58** (1940) 371.
79. *Idem. Trans. AIME* **143** (1941) 30.
80. J. S. KOEHLER, in "Imperfections in Nearly Perfect Crystals", edited by W. Shockley (Wiley, New York, 1952) pp. 197–215.
81. K. LÜCKE and A. V. GRANATO, in "Dislocations and

Mechanical Properties of Crystals" (Wiley, New York, 1956) pp. 425–57.
82. A. V. GRANATO, in "Dislocations and Properties of Real Materials" (The Institute of Metals, London, 1985). pp. 266–82.
83. D. H. ROGERS, *J. Appl. Phys.* **33** (1962) 781.
84. A. WOLFENDEN, M. R. HARMOUCHE and S. V. HAYES, in "Testing Technology of Metal Matrix Composites", ASTM STP 964, edited by P. R. DiGiovanni and N. R. Adsit (ASTM, Philadelphia, PA, 1988) pp. 207–15.
85. J. E. HATCH, "Aluminum, Properties and Metallurgy" (ASM, Metals Park, OH, 1984) pp. 143–4.

Received 11 February
and accepted 7 April 1992